Journal of Sound and Vibration (2001) **241**(3), 373–399
doi:10.1006/jsvi.2000.3310, available online at http://www.idealibrary.com on IDEAL®

BOUNDARY CONDITION ERROR FOR PARAMETRIC UPDATING OF IN-OPERATION SYSTEMS—APPLICATION TO PIPING SYSTEMS

S. FRIKHA

Laboratoire de Mécanique Physique, Université Pierre et Marie Curie, CNRS, UPRES-A 7068, *France*

M. GAUDIN

*Électricité De France – Division Recherche & Développement, RNE/AMV/T*64 – 92141 *Clamart, France*

AND

G. COFFIGNAL

Laboratoire de Modélisation et de Mécanique des Structures – UPMC/ENSAM/ENS Cachan – CNRS, UPRES-A 8007, *France*

(*Received* 24 *February* 2000, *and in final form* 2 *August* 2000)

There is an increasing interest in experimental analysis of in-operation structures where a part of the boundary conditions is poorly known. This concerns particularly the case of coupled systems where some complex physical phenomena make the behaviour of both the system and its connectivity dependent on the functioning conditions. In this context, this paper presents a new frequency approach for parametric structural updating in the vibration and acoustic fields. This methodology is developed here in the case of piping systems. It follows the boundary conditions identification method previously developed by the authors. A boundary conditions error is presented and its efficiency to translate structural parameters error is shown. Thus, the proposed approach allows performing the identification of some unknown boundary conditions and, simultaneously, updating the model of the tested structure. The pertinence of a frequency choice criteria based on the smallest singular value of the solved system during the identification of the boundary conditions is shown. It specifically allows avoiding the bands of critical frequencies. The developed updating technique is tested with two actual cases: a laboratory test case and an industrial example.

1. INTRODUCTION

The vibration and acoustic control and fault diagnosis of piping systems require a confident modelling of their dynamic behaviour. To make sense, such a model must be capable of reproducing the system response under operating conditions. The strong mechanical coupling often encountered in piping networks makes their behaviour dependent on these conditions. It therefore becomes difficult to make a purely analytical model of the physical phenomena governing their behaviour. The physical knowledge has to be completed by experimental investigations. The problem to be solved consists in computing simultaneously a part of the response of a system (outputs) and a part of its inputs by combining experimental data with the analytical model. This is an inverse problem as some of the classic inputs of the system are estimated by using its classic output. It can also be

0022-460X/01/130373 + 27 $35.00/0

considered as a hybrid problem since an experimental approach is combined with an analytical approach so as to estimate more accurately the output of the system by reducing the model and the measurement errors.

In this context, the purpose of this work is to develop some useful tools for the experimental analysis performed on working systems. In many cases, this leads to a situation where some of the boundary conditions are poorly known or even totally unknown.

Initially, this problem was approached by the authors assuming that the dynamic behaviour of the tested structure was well modelled. An inverse method of boundary conditions identification has been developed [1, 2]. It specifically allows estimating the frequency spectra of generalized displacement and forces according to non-modelled boundary conditions.

This paper presents the results of the second stage of this work where the problem of improving the structure model has been addressed. The basic idea is that the identification of some well-known boundary conditions may provide a measure of the model accuracy and may be used to improve it.

First, this idea was tested in the case where all boundary conditions are well modelled [3, 4]. This consisted of a classic updating problem which has been widely treated during the last two decades [5–12]. The same approach is then extended to a more general case where only a part of the boundary conditions are defined. More recently, this kind of problem, generally referred to as an "*in-situ*" or "in-operation" experimental analysis, has been studied by several authors [13–18].

The method developed here addresses the problem of in-operation experimental analysis and is based on a new parametric updating approach by minimizing a "boundary conditions error" (BCE), in the frequency domain. The theoretical formulation is developed in the case of one-dimensional structures because of the large application field that they provide. Nevertheless, this approach may be applied to other kinds of structures.

The principle of the updating method is described in the first part; the BCE and its sensitivity according to an updating parameter are detailed. In the second part, a critical analysis is presented. Interest is focussed on the choice of the frequencies used for updating. A criterion is established in order to characterize the critical frequencies that have to be avoided. Its efficiency is shown in several examples. In the final part, some results are presented. The first example is a classic beam structure where the experimental data were numerically synthesized. The second case is a laboratory test where Young's modulus of a long steel pipe supported by poorly known supports and submitted to an unknown excitation was identified. The last example is an industrial one; it presents the result of an experimental analysis performed on a suction circuit of an energy production plant.

2. PRINCIPLE

The parametric updating approach is basically related to the boundary conditions identification method developed by the authors in reference [1]. The method which considers a part of a structure subjected to experimental analysis, consists in building and inverting the transfer relation between the measured structure response and the boundary conditions that have to be identified (see Figure 1). It therefore requires a good knowledge of the mechanical characteristics of the tested system. As an example, it is shown in reference [2] that the accuracy of a force identification acting on a straight beam is strongly affected by a wrong estimation of the beam's Young's modulus. Indeed, the tested structure may be seen as a generalized "macro-sensor" allowing an experimental assessment of unknown

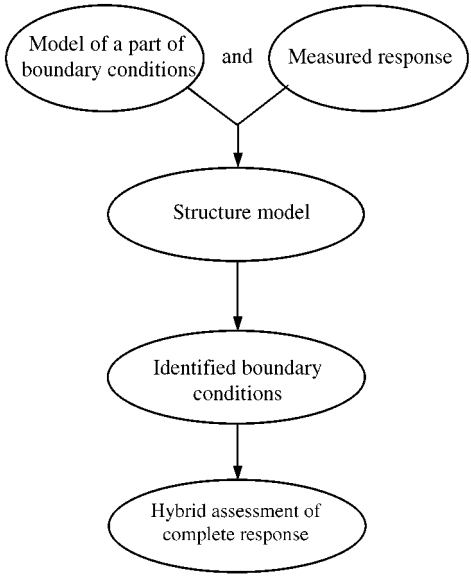

Figure 1. Boundary condition identification algorithm.

boundary conditions. Like any measuring device, it has to be accurately calibrated. In other words, the dynamic behaviour of this macro-sensor has to be confidently reproduced by a mathematical model providing the correct relation between direct observations (measured response) and the unknowns addressed by the measurements (identified boundary conditions). Thus, as it is used to calibrate a measuring instrument by using a standard device, the basic idea of the updating method presented here is to calibrate the model idealizing the dynamic behaviour of the so-called "macro-sensor" by applying some well-known boundary conditions to it. From a formal point of view, the updating is carried out by minimizing an objective function expressed in terms of a set of structural parameters (geometrical or mechanical). This function is a measure of the error made during the identification of a set of boundary conditions here called "test boundary conditions". It is postulated here that this boundary condition error gives a mapping from structural parameters space to boundary conditions space and that this mapping is injective. The accuracy of the updated model is assumed to be characterized by this error: it reaches its maximum when this error reaches its minimum.

This section begins with a short recall of the boundary identification method and a basic presentation of the boundary condition error. The detailed construction of this error and its derivative with respect to an updating parameter is then presented. Finally, the particular case where test degrees of freedom (d.o.f.s) and measured degrees of freedom are merged, is detailed.

2.1. RECALL OF THE BOUNDARY CONDITION IDENTIFICATION METHOD

The method of boundary conditions identification [2] is the starting point of the updating approach presented in this paper. It is a frequency domain method. One-dimensional structures composed of beams, fluid-filled pipes and lumped elements constitute its main field of application. Such structures are modelled by using continuous

TABLE 1

Boundary condition types for the problem of boundary conditions identification

Boundary condition	Generalized displacement	Generalized force
Link	Will be identified: $\{q_l\}$	Will be identified: $\{Q_l\}$
Imposed or clamped	Model data: $\{q_c\}$	Unknown: $\{Q_c\}$
Free or source	Unknown: $\{q_f\}$	Model data: $\{Q_f\}$

elements connected by nodes which support all its degrees of freedom.† Unlike the finite element models, this formulation does not require a fine mesh. Indeed, nodes are defined only at points where there is a geometrical or mechanical singularity and at points where the structure is linked to the exterior.

Only a part of the boundary conditions is modelled. Table 1 summarizes the types of degrees of freedom. In addition to the classic "source" and "clamped" boundary conditions, there is a new type referring to unknown boundary conditions denoted here by "link degrees of freedom" and noted with the subscript l. In order to overcome the ill-conditioned nature of the problem, some measurements of the structure response are made on the nodes or inside the elements. By using a transfer matrix formulation, a global transfer relation, expressing these measurements in terms of all degrees of freedom, is created.

The unknowns of the boundary conditions identification problem are as follows: $\{q_l\}$: generalized displacements at an unknown boundary; $\{Q_l\}$: generalized forces at an unknown boundary.

A condensation of all degrees of freedom having well-known boundary conditions is performed, so that the model of the structure is reduced to link degrees of freedom $\{q_l\}$. For each frequency, the following equations are obtained:

$$\{C(\omega)\} = [T_s(\omega)]\{q_l(\omega)\} + \{\bar{C}(\omega)\}, \tag{1}$$

$$\{Q_l(\omega)\} = [Z_l(\omega)]\{q_l(\omega)\} + \{\bar{Q}_l(\omega)\}. \tag{2}$$

Here $\{C\}$ contains the experimental data, $[Z_l]$ is a dynamic stiffness matrix and $[T_s]$ is the measurement transfer matrix. The terms $\{\bar{C}\}$ and $\{\bar{Q}_l\}$ are derived from the condensation of the degrees of freedom having a known boundary condition (source and clamped); they are expressed as functions of $\{q_c\}$ and $\{Q_f\}$. In order to obtain a full-ranked system, the number of sensors must be equal or higher than the number of unknown boundary conditions:

$$size\{C\} \geqslant size\{q_l\}. \tag{3}$$

Solving equation (1) leads to an assessment of the generalized displacements $\{q_l\}$,

$$\{q_l\}_{(\omega)} = [T_s]^+(\{C\} - \{\bar{C}\}), \tag{4}$$

where $[T_s]^+$ is the generalized inverse of $[T_s]$. Substituting $\{q_l\}$ into equation (2) leads to an estimation of the generalized forces $\{Q_l\}$:

$$\{Q_l\}_{(\omega)} = [Z_l][T_s]^+(\{C\} - \{\bar{C}\}) + \{\bar{Q}_l\}. \tag{5}$$

† Here we deal with continuous models, so, in the literal sense, the number of degrees of freedom is infinite. We will use this denomination to refer to the boundary degrees of freedom which have a finite number, thus continuous sources are excluded.

This task is performed for each frequency and characterizes the unknown boundary conditions allowing the computation of the frequency response of the whole structure. A list of nomenclature is given in Appendix B.

2.2. BOUNDARY CONDITIONS ERROR (BCE)

The principle of structural updating is based on the improvement of the tested structure model being used for the identification of the link boundary conditions. It is assumed here that the precision of the model is correlated to the precision of the boundary conditions identification. It is proposed here to check and then to improve its quality by identifying some given forces and/or displacements in areas where they are well known. The degrees of freedom used for this purpose are here called "test degrees of freedom" and denoted $\{q_t\}$. These degrees of freedom are a subgroup of the actually clamped and source (or free) degrees of freedom: $\{q_t\} = \{q_{tc}\ \ q_{tf}\} \subset \{q_c\ \ q_f\}$. The associated forces are denoted by

$$\{Q_t\} = \{Q_{tc} \quad Q_{tf}\}.$$

Globally, the structure's degrees of freedom are classified as in Table 2. Equations (4) and (5) therefore become

$$\begin{Bmatrix} q_l \\ q_t \end{Bmatrix}_{(p,\omega)} = [T_s(p,\omega)]^+(\{C(\omega)\} - \{\bar{C}(p,\omega)\}), \tag{6}$$

$$\begin{Bmatrix} Q_l \\ Q_t \end{Bmatrix}_{(p,\omega)} = \begin{bmatrix} Z_l(p,\omega) \\ Z_t(p,\omega) \end{bmatrix} [T_s(p,\omega)]^+(\{C(\omega)\} - \{\bar{C}(p,\omega)\}) + \begin{Bmatrix} \bar{Q}_l(p,\omega) \\ \bar{Q}_t(p,\omega) \end{Bmatrix}. \tag{7}$$

The identified forces $\{Q_{tf}\}$ and displacement $\{q_{tc}\}$ are explicitly dependent on the parameters $\{p\}$ of the analytical model. They should be compared with the well-known forces $\{\hat{Q}_{tf}\}$ and the well-known displacements $\{\hat{q}_{tc}\}$. A complex error vector is then defined as being the algebraic deviation between the identified quantities and those known,

$$\{\varepsilon(p,\omega)\} = \begin{Bmatrix} \{Q_{tf}(\omega,p) - \hat{Q}_{tf}(\omega)\} \\ \{q_{tc}(\omega,p) - \hat{q}_{tc}(\omega)\} \end{Bmatrix}, \tag{8}$$

where $\lfloor W_q \rfloor$ is a displacement weighting matrix and $\lfloor W_Q \rfloor$ is a force weighting matrix, so as to homogenize the dimensions and the orders of magnitude of the error vector components.

TABLE 2

Boundary conditions types for the problem of updating a structure having unknown boundary conditions

Boundary condition		Generalized displacement	Generalized force
Identified	Link	Unknown: $\{q_l\}$	Unknown: $\{Q_l\}$
	Test	Tested: $\{q_{tc}\} = \{\hat{q}_{tc}\}$	Unknown: $\{Q_{tc}\}$
		Unknown: $\{q_{tf}\}$	Tested: $\{Q_t\} = \{\hat{Q}_{tf}\}$
Imposed or clamped		Model data: $\{q_c\}$	Unknown: $\{Q_c\}$
Free or source		Unknown: $\{q_f\}$	Model data: $\{Q_f\}$

The error defined in equation (8) is calculated for a set of angular frequencies $\{\omega_1, \ldots, \omega_n\}$, the objective function $\varphi(p)$ being defined as the norm of the global error vector obtained by gathering the errors of all the angular frequencies $\{\omega_1, \ldots, \omega_n\}$,

$$\varphi(p) = \left\| \begin{matrix} \| \varepsilon(p, \omega_1) \|_{[W_q], [W_Q]} \\ \cdots \\ \| \varepsilon(p, \omega_n) \|_{[W_q], [W_Q]} \end{matrix} \right\|_{[W_\omega]}, \tag{9}$$

where $\lfloor W_q \rfloor$ is a displacement weighting matrix and $\lfloor W_Q \rfloor$ is a force weighting matrix, so as to homogenize the dimensions and the orders of magnitude of the error vector components. $[W_\omega]$ is a frequency weighting matrix.

The problem of parametric updating consists in looking for parameter values, p_{up}, verifying "as closely as possible" the following equation:

$$\text{find } p_{up} \quad \text{such that} \quad \varphi(p_{up}) = 0. \tag{10}$$

p_{up} are then called the updated parameters. Supposing the error $\varphi(p)$ takes into account all the errors of the analytical model, the forces and displacements of the actually unknown boundary conditions are computed by

$$\begin{Bmatrix} q_l \\ q_t \end{Bmatrix} = [T_s(p_{up}, \omega)]^+ (\{C\} - \{\bar{C}(p_{up})\}), \tag{11}$$

$$\{Q_l\} = [Z_l(p_{up})][T_s(p_{up})]^+ (\{C\} - \{\bar{C}(p_{up})\}) + \{\bar{Q}_l(p_{up})\}. \tag{12}$$

This procedure simultaneously allows the updating of the tested structure analytical model and the identification of its unknown boundary conditions.

2.3. CALCULATION OF THE ERROR AND ITS JACOBIAN

The construction of the objective function $\varphi(p)$ uses a formalism similar to that developed by the first author in reference [1]. As the structure is composed of elements connected by nodes, two levels of construction are found, in the typically classic manner: the elementary level and the global level.

Otherwise, as $\varphi(p)$ is generally not linear, its minimization is performed by using an optimization method based on a quadratic approximation, as a Gauss–Newton method [22]. This therefore is an iterative method requiring, for each frequency and each iteration, the computation of the gradient of $\{\varepsilon(p, \omega)\}$:

$$S(p, \omega) = \frac{\partial \varepsilon(p, \omega)}{\partial p} = \begin{Bmatrix} \dfrac{\partial Q_{tf}}{\partial p} \\ \dfrac{\partial q_{tc}}{\partial p} \end{Bmatrix}. \tag{13}$$

$S(p, \omega)$ is called the sensitivity matrix.

As for the error construction, the algorithm used for the calculation of the sensitivity matrix also comprises an elementary and a global level, both will be presented later in this section.

2.3.1. *Elementary level*

The elementary matrices computed at this level describe the dynamic behaviour of each element by means of a dynamic stiffness matrix. The transfer relation between each sensor of the element and the generalized displacement of its extremities is also expressed similarly. This yields:

$$\begin{Bmatrix} Q_e \\ C_e \end{Bmatrix}_{(\omega)} = \begin{bmatrix} Z_e \\ T_{se} \end{bmatrix}_{(p,\omega)} \{q_e\}_{(\omega)}, \tag{14}$$

where $\{q_e\}$ are the element's degrees of freedom, $\{Q_e\}$ are the associated generalized forces (forces and moments applied to its extremities or acoustic flux entering through its extremities), $[Z_e]$ is the element dynamic stiffness matrix and $\{C_e\}$ is the measurement vector performed on the element at any location. The matrix $[T_{se}]$ is derived from the transfer matrix relating the sensor section state vector to the upstream element extremity. For continuous curvilinear elements, equation (14) is expressed analytically and is derived from the exact solution of the motion equation. Its differentiation relative to a mechanical or a geometrical parameter p_k is also obtained analytically. This leads to the exact partial derivatives of $[Z_e]$ and $[T_{se}]$.

2.3.2. *Global level*

The gathering of all the structure's elements is performed by expressing the continuity and the conservation laws at each node. In a classic manner, that leads to an assembling guide for each element like those used in a finite element method. Therefore, a global relation is obtained,

$$\begin{Bmatrix} Q \\ C \end{Bmatrix}_{(\omega)} = \begin{bmatrix} Z_g \\ T_{sg} \end{bmatrix}_{(p,\omega)} \{q_e\}_{(\omega)}, \tag{15}$$

where $\lfloor Z_g \rfloor$ is the dynamic stiffness matrix of the whole structure, and $\lfloor T_{sg} \rfloor$ is the measurement global transfer matrix relating the measured response to all degrees of freedom.

In a strictly analogous manner and by using the same assembling guides, partial derivatives of matrices $\lfloor Z_g \rfloor$ and $\lfloor T_{sg} \rfloor$ are obtained.

The boundary conditions are defined for each degree of freedom as shown in Table 2. Degrees of freedom are sorted according to their type of boundary conditions so that equation (15) becomes

$$\begin{Bmatrix} Q_l \\ Q_t \\ Q_f \\ Q_c \\ C \end{Bmatrix} = \begin{bmatrix} Z_{ll} & Z_{lt} & Z_{lf} & Z_{lc} \\ Z_{tl} & Z_{tt} & Z_{tf} & Z_{tc} \\ Z_{fl} & Z_{ft} & Z_{ff} & Z_{fc} \\ Z_{cl} & Z_{ct} & Z_{cf} & Z_{cc} \\ T_{sl} & T_{st} & T_{sf} & T_{sc} \end{bmatrix} \begin{Bmatrix} q_l \\ q_t \\ q_f \\ q_c \end{Bmatrix}. \tag{16}$$

The elimination of $\{q_f\}$ and $\{q_c\}$ leads to equations similar to equations (4) and (5) where the subscript l is replaced by subscripts l and t, giving

$$\begin{bmatrix} Z_l \\ Z_t \\ T_s \end{bmatrix} = \begin{bmatrix} Z_{ll} & Z_{lt} \\ Z_{tl} & Z_{tt} \\ T_{sl} & T_{st} \end{bmatrix} - \begin{bmatrix} Z_{lf} \\ Z_{tf} \\ T_{sf} \end{bmatrix} [Z_{ff}]^{-1} [Z_{fl} \quad Z_{ft}] \tag{17}$$

and

$$\begin{bmatrix} \bar{Q}_l \\ \bar{Q}_t \\ \bar{C} \end{bmatrix} = \begin{bmatrix} Z_{lc} \\ Z_{tc} \\ T_{sc} \end{bmatrix} \{q_c\} + \begin{bmatrix} Z_{lf} \\ Z_{tf} \\ T_{sf} \end{bmatrix} [Z_{ff}]^{-1} (\{Q_f\} - [Z_{fc}]\{q_c\}). \tag{18}$$

Recalling the composition of the test degrees of freedom $\{q_t\}^t = \{q_{tf} \;\; q_{tc}\}^t$, the error vector will therefore be written as

$$\varepsilon(p,\omega) = \begin{Bmatrix} [1_{tf} \;\; 0_{tc}][Z_t][T_s(p,\omega)]^+(\{C\} - \{\bar{C}\}) + \{\bar{Q}_{tf}\} - \{\hat{Q}_{tf}\} \\ [0_l \;\; 0_{tf} \;\; 1_{tc}][T_s(p,\omega)]^+(\{C\} - \{\bar{C}\}) - \{\hat{q}_{tc}\} \end{Bmatrix}, \tag{19}$$

where $\lfloor 1_{tf} \;\; 0_{tc} \rfloor$ extracts $\{q_{tf}\}$ from the test degrees of freedom $\{q_t\}$ and $\lfloor 0_l \;\; 0_{tf} \;\; 1_{tc} \rfloor$ extract $\{q_{tc}\}$ from the identified degrees of freedom $\{q_l \;\; q_t\}$. The terms intervening in the computation of the sensitivity matrix defined in equation (13) are

$$\begin{aligned} \left\{\frac{\partial Q_{tf}}{\partial p}\right\} = {} & [1_{tf} \;\; 0_{tc}] \left[\frac{\partial Z_t}{\partial p}\right] [T_s]^+(\{C\} - \{\bar{C}\}) \\ & - [1_{tf} \;\; 0_{tc}][Z_t][T_s]^+ \frac{\partial [T_s]}{\partial p} [T_s]^+(\{C\} - \{\bar{C}\}) \\ & - [1_{tf} \;\; 0_{tc}][Z_t][T_s]^+ \left\{\frac{\partial \bar{C}}{\partial p}\right\} + \left\{\frac{\partial \bar{Q}_{tf}}{\partial p}\right\}, \end{aligned} \tag{20}$$

$$\begin{aligned} \left\{\frac{\partial q_{tc}}{\partial p}\right\} = {} & - [0_l \;\; 0_{tf} \;\; 1_{tc}][T_s]^+ \frac{\partial [T_s]}{\partial p} [T_s]^+(\{C\} - \{\bar{C}\}) \\ & - [0_t \;\; 0_{tf} \;\; 1_{tc}][T_s]^+ \left\{\frac{\partial \bar{C}}{\partial p}\right\} \end{aligned} \tag{21}$$

with

$$\begin{aligned} \begin{bmatrix} \dfrac{\partial Z_t}{\partial p} \\ \dfrac{\partial T_s}{\partial p} \end{bmatrix} = {} & \begin{bmatrix} \dfrac{\partial Z_{tl}}{\partial p} & \dfrac{\partial Z_{tt}}{\partial p} \\ \dfrac{\partial T_{sl}}{\partial p} & \dfrac{\partial T_{st}}{\partial p} \end{bmatrix} - \begin{bmatrix} \dfrac{\partial Z_{tf}}{\partial p} \\ \dfrac{\partial T_{sf}}{\partial p} \end{bmatrix} [Z_{ff}]^{-1} [Z_{fl} \quad Z_{ft}] \\ & + \begin{bmatrix} Z_{tf} \\ T_{sf} \end{bmatrix} [Z_{ff}]^{-1} \frac{\partial [Z_{ff}]}{\partial p} [Z_{ff}]^{-1} [Z_{fl} \quad Z_{ft}] \\ & - \begin{bmatrix} Z_{tf} \\ T_{sf} \end{bmatrix} [Z_{ff}]^{-1} \begin{bmatrix} \dfrac{\partial Z_{fl}}{\partial p} & \dfrac{\partial Z_{ft}}{\partial p} \end{bmatrix} \end{aligned} \tag{22}$$

and

$$\begin{Bmatrix} \dfrac{\partial \bar{Q}_t}{\partial p} \\ \dfrac{\partial \bar{C}}{\partial p} \end{Bmatrix} = \begin{bmatrix} \dfrac{\partial Z_{tc}}{\partial p} \\ \dfrac{\partial T_{sc}}{\partial p} \end{bmatrix} \{q_c\} + \begin{bmatrix} \dfrac{\partial Z_{tf}}{\partial p} \\ \dfrac{\partial T_{sf}}{\partial p} \end{bmatrix} [Z_{ff}]^{-1} \{Q_f - Z_{fc} q_c\}$$

$$- \begin{bmatrix} Z_{tf} \\ T_{sf} \end{bmatrix} [Z_{ff}]^{-1} \frac{\partial Z_{ff}}{\partial p} [Z_{ff}]^{-1} \{Q_f - Z_{fc} q_c\}$$

$$- \begin{bmatrix} Z_{tf} \\ T_{sf} \end{bmatrix} [Z_{ff}]^{-1} \left\{ \frac{\partial Z_{fc}}{\partial p} q_c \right\}, \tag{23}$$

where it should be recalled that $\partial \bar{Q}_{tf}/\partial p = [1_{tf} \;\; 0_{tc}] \partial \bar{Q}_t/\partial p$ and that the derivative of the generalized inverse of a matrix $[A]$ is obtained by using the relationship

$$\frac{\partial [A]^+}{\partial p} = - [A]^+ \frac{\partial [A]}{\partial p} [A]^+.$$

2.4. A SPECIAL CASE OF STRUCTURAL UPDATING WITHOUT UNKNOWN BOUNDARY CONDITIONS

The only explicit constraint when choosing the test degrees of freedom is that their number is limited by the fact that an overabundance of sensors is needed. This maximum number is equal to the difference between the number of sensors and the number of link degrees of freedom. When all the boundary conditions are modelled, this is again a classic updating problem without any link degrees of freedom. The procedure of boundary conditions identification then concerns only the test degrees of freedom. Their number may be equal to that of the sensors.

A special case which would be interesting to develop is when the sensors and the test degrees of freedom are merged: $\{q_t\} = \{q_{tf}\} = \{C\}$.

In other words, q_{tc} and q_l do not exist and the measurements are made according to some free degrees of freedom, and the identification of associated external generalized forces (well known and generally equal to zero), is used to build the objective function. This leads to $\{Q_t\} = \{Q_{tf}\}$.

The matrix $[T_s]$ is then an identity matrix and its derivative equals zero:

$$[T_s] = [1_t], \qquad [\partial T_s/\partial p] = [0_t].$$

The error expression becomes

$$\{\varepsilon(p, \omega)\} = \{Q_t\}_{(p,\omega)} - \{\hat{Q}_t\} = [Z_t(p, \omega)]\{C(\omega)\} + \{\bar{Q}_t(p, \omega)\} - \{\hat{Q}_t\} \tag{24}$$

with

$$[Z_t] = [Z_{tt}] - [Z_{tf}][Z_{ff}]^{-1}[Z_{ft}],$$

$$\{\bar{Q}_t\} = [Z_{tf}][Z_{ff}]^{-1}\{Q_f\} + ([Z_{tc}] - [Z_{tf}][Z_{ff}]^{-1}[Z_{fc}])\{q_c\}. \tag{25}$$

As the matrix $[T_s]$ is an identity matrix, the computation of the objective function thereby requires only the inversion of the dynamic stiffness matrix $\lfloor Z_{ff} \rfloor$. On the other hand, the

estimation of the objective function is obtained without overabundant information, which implies that at the stage of error computation, the measurement noise is not averaged. This therefore will tend to show a strong sensitivity to measurement noise, especially when the matrix $\lfloor Z_{ff} \rfloor$ is poorly conditioned. It is, however, worth noting that the experimental information can be averaged during the minimization of the objective function.

3. CRITICAL ANALYSIS OF THE OBJECTIVE FUNCTION

Just as the modelled errors here are assumed well located, the choice of the test degrees of freedom is also left to the user. It is quite evident that this choice is extremely important for the success of the updating process. In fact, it is necessary for the test boundary conditions to be sensitive to the value of the targeted updating parameter. This requires an advanced understanding of the physics of the system and some expertise of the structure modelling. These two choices are here assumed to be fixed and we turn towards the choice of experimental data used for the structural updating.

It is well known that the more an objective function is regular and convex, the more simple is its min–max investigation. These properties become crucial when solving a non linear optimization problem by using a technique so that the search direction is obtained by the gradient estimation and the step length is estimated according to a local approximation. Close to some frequencies, some of the terms involved in the calculation of $\varepsilon(p, \omega)$ may present large variations leading to frequency peaks that may be very sharp, especially when the damping is weak. When these frequencies depend on the updating parameters, this singular behaviour is associated with a parameter neighbourhood. The singularity of the objective function observed on the frequency axis also becomes a singularity on the parameter axis. The gradient of the objective function tends to infinity.

3.1. CRITICAL FREQUENCY BANDS

Bearing in mind the expression of $\varepsilon(p)$, such behaviour can be observed only if the linear system given by equation (16) becomes almost singular. Omitting the equations associated with an unknown left-hand side member, and gathering the identified boundary conditions under the subscript u, one finds that the system actually solved is

$$\begin{Bmatrix} C \\ Q_f \end{Bmatrix} = \begin{bmatrix} T_{su} & T_{sf} & T_{sc} \\ Z_{fu} & Z_{ff} & Z_{fc} \end{bmatrix} \begin{Bmatrix} q_u \\ q_f \\ q_c \end{Bmatrix}. \tag{26}$$

Reducing the data $\{q_c\}$ to the second member, give

$$\begin{Bmatrix} C - T_{sc} q_c \\ Q_f - Z_{fc} q_c \end{Bmatrix} = \begin{bmatrix} T_{su} & T_{sf} \\ Z_{fu} & Z_{ff} \end{bmatrix} \begin{Bmatrix} q_u \\ q_f \end{Bmatrix}. \tag{27}$$

Let T_{suf} denote the matrix corresponding to this system.

The resolution of this system is decomposed in two stages. The first consists in expressing $\{q_f\}$ as a function of $\{q_u\}$, the second consists in solving the system obtained in $\{q_u\}$. The determinant of the matrix T_{suf} can therefore be written in the form of a product of the

determinants of the submatrix Z_{ff} and the condensed transfer matrix T_s:

$$\det(T_{suf}) = \begin{vmatrix} I_{ss} & T_{sf} \\ 0 & Z_{ff} \end{vmatrix} \begin{vmatrix} T_{su} - T_{sf} Z_{ff}^{-1} Z_{fu} & 0 \\ Z_{ff}^{-1} Z_{fu} & I_{ff} \end{vmatrix}$$

$$= \det(Z_{ff}) \det(\underbrace{T_{su} - T_{sf} Z_{ff}^{-1} Z_{fu}}_{=T_s}). \tag{28}$$

Let ω_s denote a pulsation near where the matrix T_s tends towards a singular matrix and ω_f a pulsation near where the matrix Z_{ff} tends towards a singular matrix. With the reservation that Z_{fu} and T_{sf} are not equal to zero and that the submatrix T_{su} is finite, one finds

$$\lim_{\omega \to \omega_f} T_s = \lim_{\omega \to \omega_f} \left(T_{su} - \frac{1}{\det(Z_{ff})} [T_{sf}][\text{Cofactor}(Z_{ff})]^{\mathrm{T}} [Z_{fu}] \right)$$

$$= \lim_{\omega \to \omega_f} \frac{1}{\det(Z_{ff})} [T_{sf}][\text{Cofactor}(Z_{ff})]^{\mathrm{T}} [Z_{fu}]. \tag{29}$$

This implies that

$$\lim_{\omega \to \omega_f} |\det(T_{suf})| = \lim_{\omega \to \omega_f} |\det(Z_{ff}) \det(T_{su} - T_{sf} Z_{ff}^{-1} Z_{fu})| > 0. \tag{30}$$

From this, one can deduce that if Z_{fu} and T_{sf} are not identically equal to zero, the matrix T_{suf} does not tend towards a singular matrix near ω_f and that it becomes singular only near ω_s:

$$\lim_{\omega \to \omega_f} \det(T_{suf}) = 0.$$

On the other hand, if Z_{fu} or T_{sf} are equal to zero, the singularity of the matrix T_{suf} becomes synonymous with the singularity of Z_{ff} or T_{su}. Especially if the rank of T_{su} is equal to the number of identified boundary condition, T_{suf} becomes singular only near frequencies ω_f:

$$\text{if } (T_{sf} = 0 \text{ or } Z_{fu} = 0) \quad \text{then } \lim_{\omega \to \omega_f} \det(T_{suf}) = 0.$$

Two types of singularities can then be encountered: Type 1: $[T_s]$ is singular; Type 2: $\lfloor T_{sf} \rfloor = [0]$ or $\lfloor Z_{fu} \rfloor = [0]$ and $\lfloor Z_{ff} \rfloor$ is singular.

The corresponding frequencies are called here "critical frequencies". The first type of singularity corresponds to a configuration where the sensors do not allow the observation of the identified displacements $\{q_u\}$. Near the corresponding frequencies, the experimental data become linearly dependent. This is a problem concerning a lack of information on which to base the optimization of sensor placement or the use of overabundant sensors. In addition, as the couples (p, ω) near where this kind of singularity occurs depend also on the choice of the test degrees of freedom, another solution can be the reduction of their number so as to remove the singularity.

The second type of singularity occurs near the couples (p, ω) where ω is an eigenfrequency of the structure, parameterized by current $\{p\}$, clamped at all identified degrees of freedom $\{q_u\}$. In fact, $\lfloor Z_{ff} \rfloor$ is the dynamic stiffness matrix of the current structure having $\{q_f\}$ as

only generalized co-ordinates. At the corresponding eigenmodes, a slight variation in the identified displacement $\{q_u\}$ results in a major change in the identified forces $\{Q_u\}$. To explain this, it is enough to recall that an eigenmode may be excited by imposing on clamped degrees of freedom a given harmonic fluctuation of the pulsation equal to the corresponding eigenfrequency. This type of singularity is notably encountered if the sensors are merged with the test degrees of freedom (cf. section 2.4) or if the measurements are explicitly expressed (without condensation) as a function of link and test degrees of freedom only. It is clear that the singularity of the objective function is all the more bothersome as the measurements become noisy. In both cases presented above, the use of additional measurements allows the reduction of the effects of measurement noise. In fact, in the first case, this will increase the number of rows of matrix $[T_s]$ and, in this way improve its ranking. In the second configuration (where the dimension of $\{q_u\}$ equals the number of measurements), this allows an increase in the number of test degrees of freedom which shifts critical frequencies towards the higher ones.

Otherwise, as with all behaviour associated with a resonance, the presence of damping flattens the peaks of the objective function around the critical couples (p, ω) thereby softening the singularity and at the same time widening its spectrum.

3.2. EXAMPLES

So as to illustrate these singularities, consider the simple case of a straight beam of length unity, joined to the ground by two transverse slides at its extremities (see Figure 2). It is excited by a transverse force at abscissa 0·4, two transverse displacement sensors are simulated at abscissas 0·4 and 0·6.

3.2.1. *First type of critical frequency band*

To highlight the first type singularity, the transverse displacements at abscissas 0·68 and 1. were chosen as test degrees of freedom. The upper graph of Figure 3 presents the determinant of matrices $\lfloor T_{suf} \rfloor$, $[T_s]$ and $\lfloor Z_{ff} \rfloor$ versus frequency. There is a clearly visible simultaneous drop in both determinants of $\lfloor T_{suf} \rfloor$ and $[T_s]$ whereas the drop in the determinant of $\lfloor Z_{ff} \rfloor$ does not induce any singularity in system (27). The graph below presents the corresponding smallest singular values and confirms the results shown in the upper one. Remember that the smallest singular value constitutes a measure of the distance between a matrix and the nearest ill-ranked matrix. In the vicinity of 24 Hz, $\lfloor Z_{ff} \rfloor$ suddenly approaches a singular matrix whereas the matrices $\lfloor T_{suf} \rfloor$ and $[T_s]$ show no particularity. However, in the vicinity of 57 Hz, they tend simultaneously towards singular matrices.

One can now observe the behaviour of the objective function. Consider as updating parameters Young's modulus of the part downstream the excitation, called here p_1 and Young's modulus of the upstream part called p_2. The upper graph of Figure 4 shows the

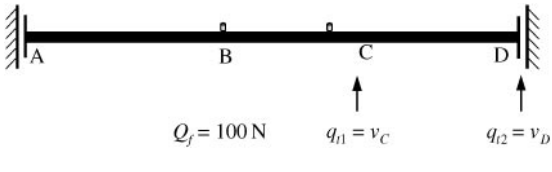

Figure 2. Schematic of the beam used to illustrate the critical frequency bands.

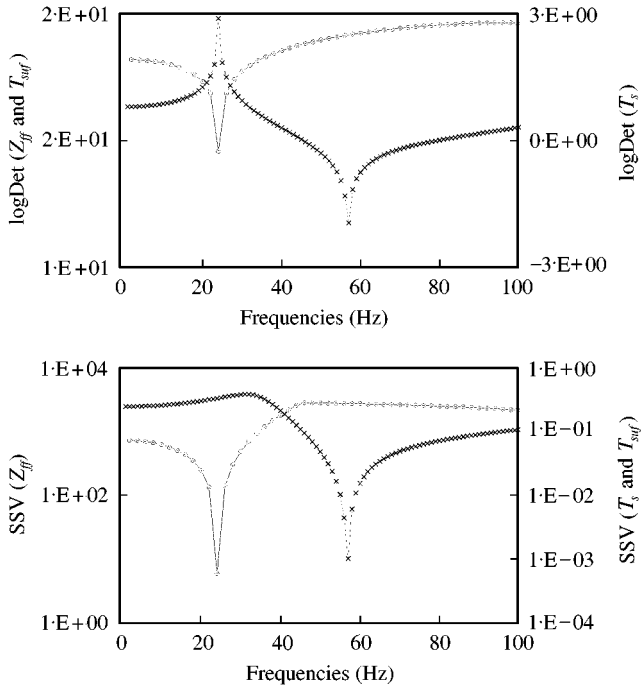

Figure 3. Determinant (upper) and smallest singular value (lower) of linear systems solved during computing the boundary condition error—Z_{ff} (circle); T_{suf} (lozenge); T_s (cross).

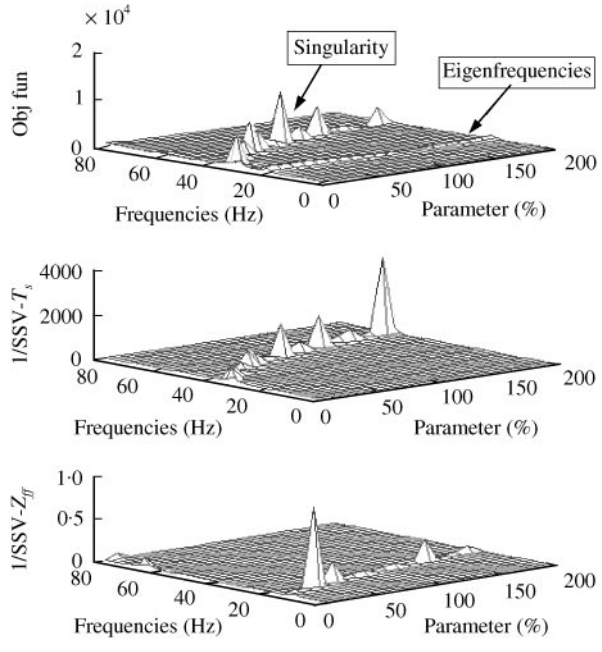

Figure 4. The norm of the vector error ε (upper) and the corresponding SSV of T_s (middle) and Z_{ff} (lower) according to the second parameter (Young's modulus of the right part) and the frequency. The sensors are located at abscissas 0·6 and 0·4 and the test degrees of freedom are the transverse displacements at abscissas 0·68 and 1. The first parameter (Young's modulus of the left part) is 20% erroneous.

evolution of the error vector norm when the parameter p_2 is maintained erroneously at -20%:

$$\| \varepsilon(p_1 \in [0{\cdot}1\, p_{1ex} \quad 2p_{1ex}],\, \omega,\, p_2 = 0{\cdot}8\, p_{2ex}) \|.$$

The graph below this figure shows the inverse of the smallest singular value of $[T_s]$ as a function of p_1 and ω. So as to better display the phenomenon to be observed, a large domain of parameters' variations is examined. The examination of the objective function highlights two regions of high gradient. The first region is parallel to the parameter axis, the gradient of the objective function relative to the updating parameter therefore remains finite and the objective function remains regular. The corresponding frequency (24 Hz) is an eigenfrequency of the tested structure; the peak of the objective function is caused by the peak of the measured frequency response. The second region is that observed in the band of frequencies [35–55] Hz. This region is not parallel to the parameter axis which results in a singular behaviour of the objective function. The examination of the smallest singular value of $[T_s]$ shows clearly that this region may be identified by where $[T_s]$ tends towards a singular matrix. On the other hand, the examination of the smallest singular value of $\lfloor Z_{ff} \rfloor$ shows clearly that there is no correlation between the singularity of the objective function and that of the matrix $\lfloor Z_{ff} \rfloor$.

3.2.2. *Second type of critical frequency band*

In order to illustrate the second type of singularity, one can merge the test degrees of freedom with the measured ones. The matrix $[T_{su}]$ becomes equal to identity. The result is shown in Figure 5 where p_2 is now taken as its exact value. A logarithmic scale is used so as to discern simultaneously the valleys and the ridges of the objective function. It must be noted that this type of representation accentuates the downward slopes towards zero and reduces those mounting towards infinity. A ridge parallel to the parameters axis is found, corresponding to the eigenfrequency of the reference structure. Additionally, two bands are discerned where $\|\varepsilon(p, \omega)\|$ increases abruptly. The first starts at 20 Hz and finishes at 70 Hz,

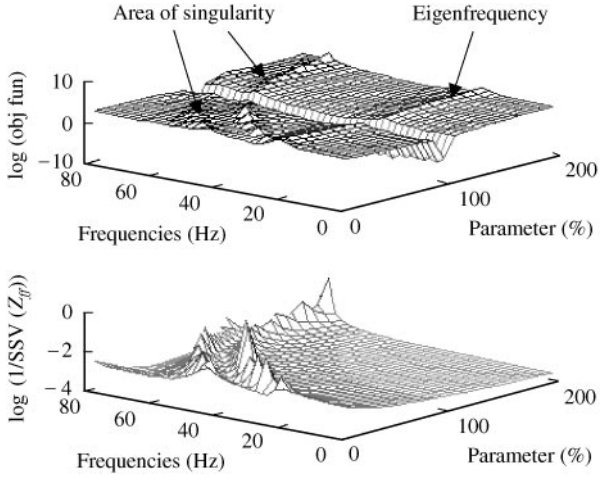

Figure 5. The norm of the vector error ε (upper) and the corresponding SSV of Z_{ff} (lower) according to the second parameter (Young's modulus of the right part) and the frequency. The sensors and the test degrees of freedom are merged and located at abscissas 0·6 and 0·4. The first parameter (Young's modulus of the left part) is not erroneous.

the second starts at 45 Hz and reaches the limit of the frequency range for a variation of p_1 of 150%. The examination of the smallest singular value of $\lfloor Z_{ff} \rfloor$ shows that the regions of singularity of the objective function are identified as being the bands (p, ω) where $\lfloor Z_{ff} \rfloor$ tends towards a singular matrix.

In other respects, the logarithmic scale representation also highlights the behaviour of the objective function in the vicinity of the solution. As the parameter p_2 is equal to its reference value, this allows to ascertain that the objective function is cancelled when p_1 is also equal to its reference value, even when crossing critical frequency areas.

4. RESULTS

4.1. BEAM STRUCTURE WITH SYNTHESIZED MEASUREMENT

The first example is a classical test case in which synthetic measurements obtained by a simulation of the response of a rigid jointed beam structure are used. The principal mechanical and geometrical characteristics of the tested structure are specified in Figure 6. Its nodes O_1 and O_2 are clamped, its first four eigenfrequencies are (41–83–128–165 Hz). It is excited by a force $\mathbf{F} = F_x \mathbf{e}_x + F_y \mathbf{e}_y$ at point C. Bi-axial sensors were simulated at nodes C and D as well as within the elements O_1A, AB, BC, DC and O_1D. Young's modulus is updated here for the horizontal bars O_1B and O_2C (parameter p_1) and the inclined bars O_1D and AC (parameter p_2).

Table 3 presents the various tested configurations. The identified degrees of freedom are maintained the same for all configurations: $\{q_u\} = \{u_C \; v_C \; u_D \; v_D\}$.

The excitation at C is considered unknown in configurations 2, 3, 5, 6 and 7, being

$$\{q_l\} = \{u_C \; v_C\}, \qquad \{q_t\} = \{u_D \; v_D\}.$$

It is considered perfectly known and the corresponding degrees of freedom are used as test ones in configurations 1 and 4, being

$$\{q_t\} = \{q_u\} = \{u_C \; v_C \; u_D \; v_D\}.$$

Otherwise, in configurations 1–3 the sensors are merged with the identified degrees of freedom; in configurations 3 and 6 the updating process crosses an area of critical frequencies and in configuration 7 two overabundant sensors are used to take out a singularity of the matrix $[T_s]$.

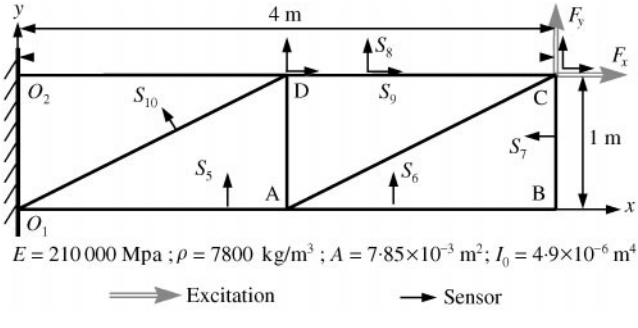

Figure 6. Schematic of the synthesized beam structure test.

TABLE 3

List of test configurations for the beam structure test

Config.	Critical freq.? freq. bands	Test d.o.f.	Link d.o.f.	Sensors
1	No/ [50:2:60] [155:2:165]	u_C–v_C–u_D–v_D	—	Four sensors merged with identified d.o.f.
2	No/ [50:2:60] [155:2:165]	u_D–v_D	u_C–v_C (excitation)	Four sensors merged with identified d.o.f.
3	Yes/ [65:5:100]	u_D–v_D	u_C–v_C (excitation)	Four sensors merged with identified d.o.f.
4	No/ [20:2:30] [165:2:175]	u_C–v_C–u_D–v_D	—	S_5–S_6–S_7–S_8
5	No/ [20:2:30] [165:2:175]	u_D–v_D	u_C–v_C (excitation)	S_5–S_6–S_7–S_8
6	Yes/ [80:5:100]	u_D–v_D	u_C–v_C (excitation)	S_5–S_6–S_7–S_8
7	No/ [80:5:100]	u_D–v_D	u_C–v_C (excitation)	S_5–S_6–S_7–S_8–S_9–S_{10} (Two overabundant sensors)

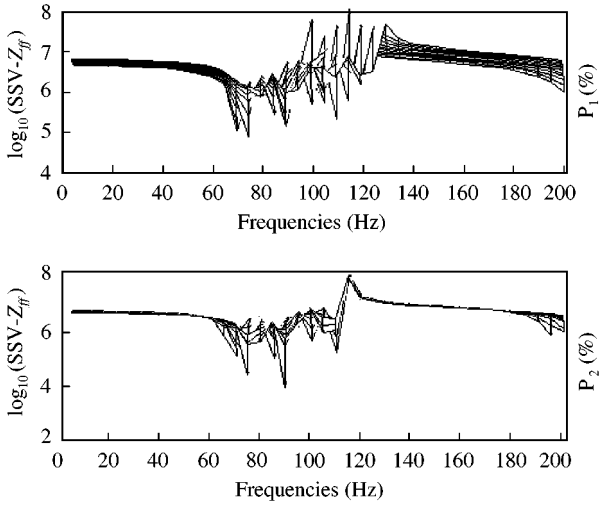

Figure 7. Smallest singular value of matrix Z_{ff} in configurations 1–3 where test degrees of freedom were merged with measured ones. Parameters are varying in a range of $\pm 25\%$ (p_1: upper, p_2: lower).

Figure 7 highlights the zones of critical frequencies for the first three configurations. The SSV of matrix $\lfloor Z_{ff} \rfloor$ are superposed as a function of the frequency for a variation of the two parameters within the limits of $\pm 25\%$. It can be seen clearly that the band of critical frequencies showing a major drop of SSV (ratio of 10^{-2}) is approximately [65–130 Hz]. Figure 8 shows the convergence of the two parameters. The hollow symbols show Young's

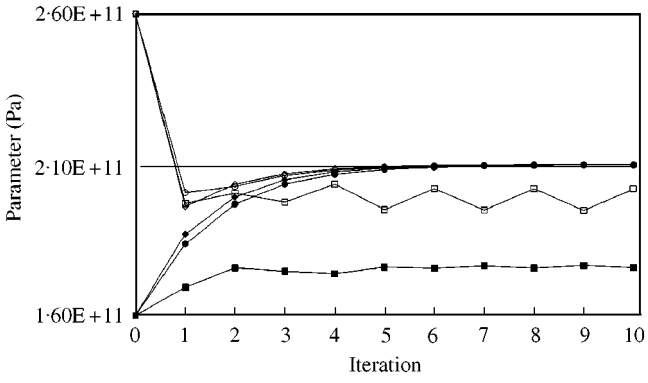

Figure 8. Convergence graph in the cases where test degrees of freedom were merged with measured ones—excitation is modelled and critical frequencies are avoided (config. 1: circle) Excitation is unknown and critical frequencies are avoided (config. 2: lozenge); Excitation is modelled and critical frequencies [65–100 Hz] are included (config. 3: square).

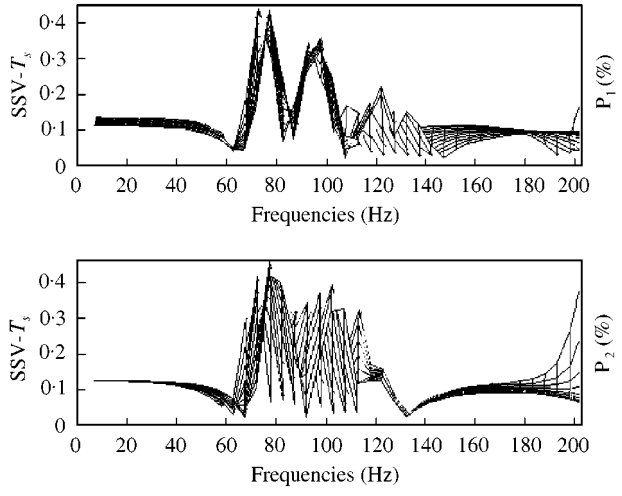

Figure 9. Smallest singular value of matrix T_s in configurations 4–6 where test degrees of freedom were not merged with measured ones. Parameters are varying in a range of $\pm 25\%$ (p_1: upper, p_2: lower).

modulus for the horizontal beams which have been initialized with 23% error ($2{\cdot}16 \times 10^5$ instead of $2{\cdot}16 \times 10^5$ MPa), and the filled symbols show Young's modulus for the inclined bars initialized with -23% error ($1{\cdot}6 \times 10^5$ instead of $2{\cdot}16 \times 10^5$ MPa). By avoiding the band of critical frequencies it is clear that both parameters converge towards their reference values. The updating process is rapid and efficient even in the presence of unknown boundary conditions. It should particularly be noted that both parameters convergence is virtually identical for configuration 1 (circle) and 2 (square). In configuration 3, the use of a set of frequencies including some critical frequencies has clearly compromised the success of the updating process. This result is as expected: on the one hand, it highlights the importance of the frequency choice; on the other, it shows, in this example, the efficiency of a frequency choice criteria based on the evolution of the SSV of $\lfloor Z_{ff} \rfloor$.

Figure 9 highlights the critical frequency zones for configurations 4–6 corresponding to a sudden drop of the SSV of $[T_s]$. Several critical frequency bands can be observed between 60 and 145 Hz. Figure 10 shows the convergence of both parameters. The statement made

earlier when commenting on the results obtained in the case where the sensors and the test degrees of freedom are merged remains valid here. It can particularly be noted that the fact of supposing the exciting force to be unknown does not at all alter the updating process. In configuration 6, the choice of a band of frequencies containing the critical frequencies [80–100 Hz] leads to an oscillation of the first parameter and a false convergence of the second. This behaviour is typical of the singularity of the objective function described in section 3. In fact, the use of critical frequencies leads to an objective function having a multitude of local minima. In the parameters space, it locally has the shape of a dish which may be very steep in one direction and very flat in another. The use of an optimization method of type Gauss–Newton method, leads to an oscillation of the parameter corresponding to the steep slope and a false convergence towards the hollow of the local minima of the parameter corresponding to the easy slope.

So as to remove the singularity from the objective function, two overabundant sensors were added in configuration 7. The matrix $[T_s]$ becomes a rectangular matrix with six rows and four columns. Figure 11 shows its SSV. It is easy to see that the band of frequencies

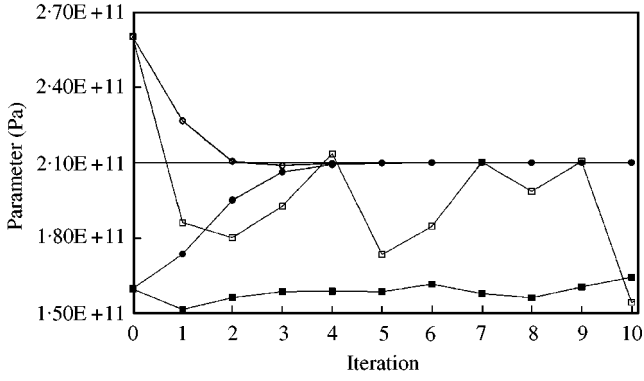

Figure 10. Convergence graph in the cases where test degrees of freedom were not merged with measured ones—excitation is modelled and critical frequencies are avoided (config. 4: circle) Excitation is unknown and critical frequencies are avoided (config. 5: lozenge, almost merged with the circles); Excitation is modelled and critical frequencies [80–100 Hz] are included (config. 6: square).

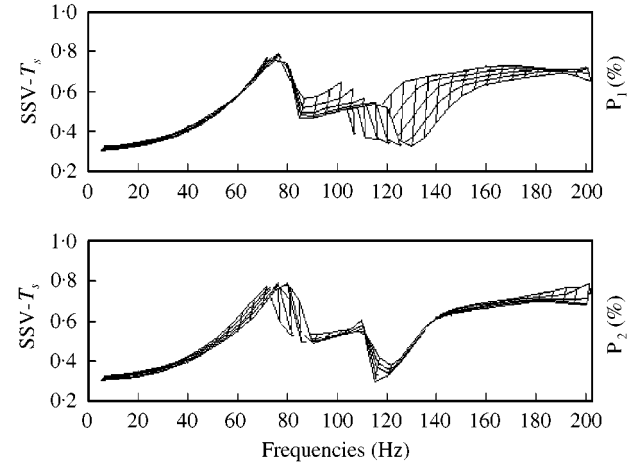

Figure 11. Smallest singular value of matrix T_s in configuration 7 where overabundant sensors were used to remove critical frequencies. Parameters are varying in a range of $\pm 25\%$ (p_1: upper, p_2: lower).

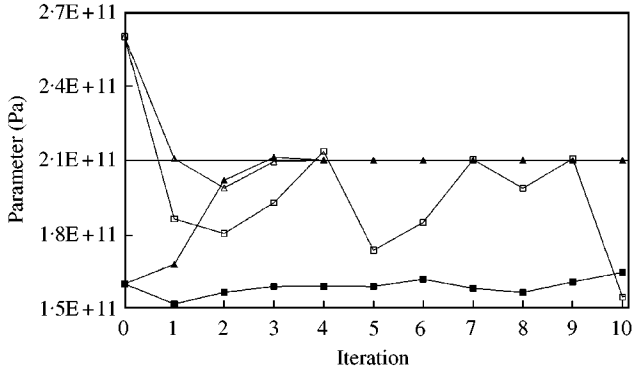

Figure 12. Convergence graph in the cases with (config. 7: triangle) and without (config. 6: square) overabundant sensors.

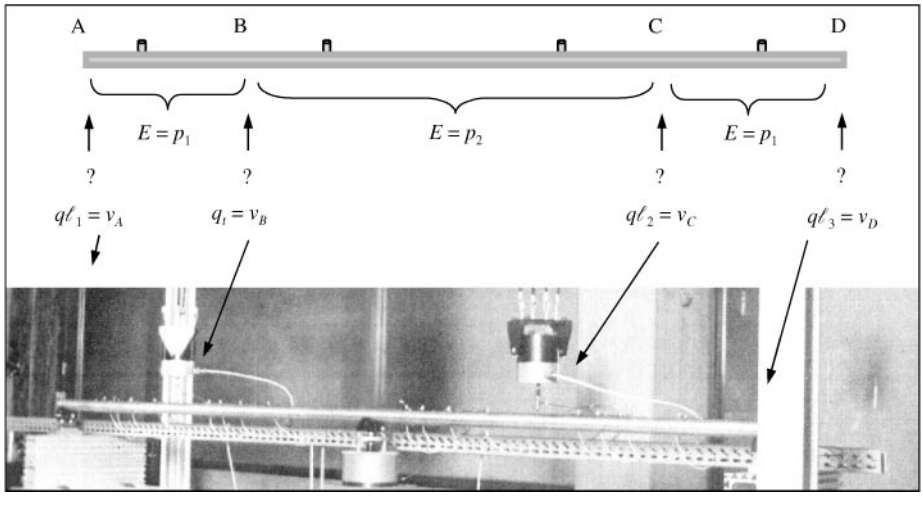

Figure 13. Schematic of the laboratory test Camelia.

[80–100] is no longer containing critical frequencies. The updating result is shown in Figure 12. The convergence of the parameters in configuration 7 is compared to that in configuration 6. It can be observed that both parameters converge towards their reference values. Otherwise, this result shows that when the sensors are not merged with the identified degrees of freedom, only the singularity of $[T_s]$ induces a singularity of the objective function which remains regular even though $\lfloor Z_{ff} \rfloor$ is singular. This result also shows the efficiency of using overabundant sensors to overcome the singularity of an objective function.

4.2. EXPERIMENTAL RESULTS OBTAINED ON A SPECIFIC TEST BENCH

Here are presented the results obtained for the updating of the mechanical characteristics of a steel pipe with unknown supports and excitation conditions. The experimental results were obtained on a laboratory test bench (see Figure 13). The tested pipe had a length of 2·895 m, it was made in stainless steel, with a diameter of 38 mm and a wall thickness of

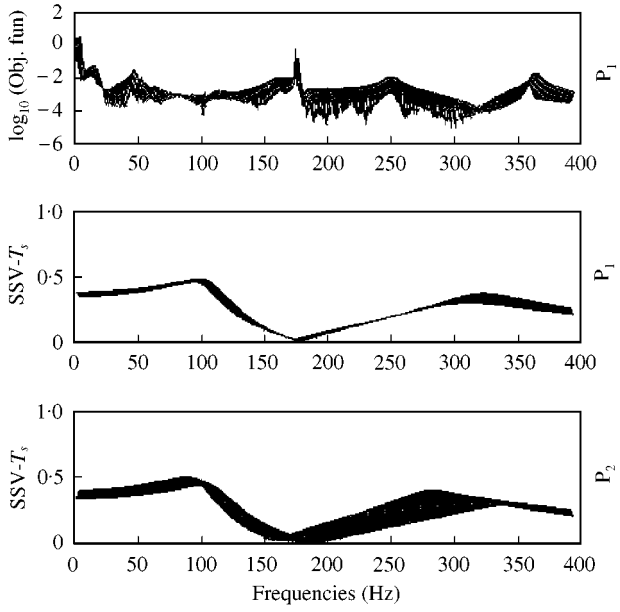

Figure 14. Objective function (upper) and smallest singular value of matrix T_s obtained for Camelia laboratory test. Parameters are varying in a range of $\pm 25\%$ (p_1: middle, p_2: lower).

2 mm. It was supported at its extremities by two flexible and dampened supports. An electrodynamic shaker, placed 2·22 m from its left end, applied a transverse force and thereby imposed a flexure motion on the pipe. Several accelerometers were placed along the pipe. The presented test used four sensors situated at abscissas {0·31, 1·01, 1·81, 2·51 m}. The exciting force was also captured and was used only for comparison with the force identification results obtained after updating. In the updated model, the pipe was divided into three parts: ([0–0·68 m]; [0·68–2·22 m]; [2·22–2·895 m]). Young's modulus for the two extreme parts was virtually supposed to be different from Young's modulus of the central part. These two moduli were initially estimated with a deliberately exaggerated error. The first was initialized at $p_{10} = 2{\cdot}3 \times 10^5$, the second at $p_{20} = 1{\cdot}6 \times 10^5$ MPa. Only the transverse displacement at the connection of the two first parts was used as a test degree of freedom. The transverse displacements corresponding to end supports and shaker force were considered as being link degrees of freedom. In other words, the supports were not modelled and the excitation was supposed to be completely unknown.

The identification of Young's moduli p_1 and p_2 is the subject of the updating procedure presented here. Figure 14 presents the evolution of the objective function and the SSV for a limit of parameter variation of 25%. A critical frequency band [150–200 Hz] is observed. The updating was then performed considering the frequencies [20 : 10 : 80 Hz] and [300 : 10 : 350 Hz]. The convergence curve is presented in Figure 15. It is shown that both parameters converge towards values near $1{\cdot}8 \times 10^5$ MPa which is a good estimation for a stainless-steel Young's modulus.

4.3. INDUSTRIAL CASE

In order to validate the approach on an industrial example, the parametric updating of the suction piping circuit presented in Figure 16 was done. The network was connected to

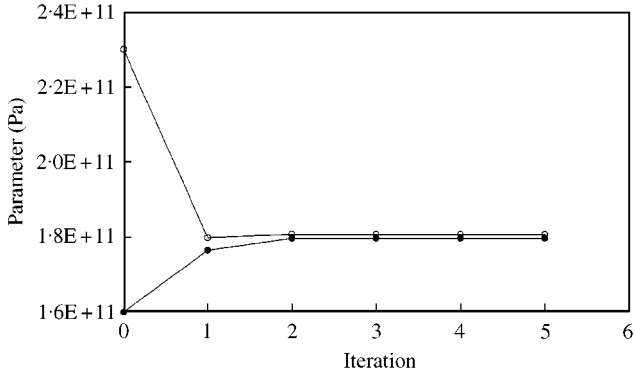

Figure 15. Convergence graph in the Camelia test case. Young's modulus of the end parts (hollow circle); Young's modulus of the middle parts (solid circle).

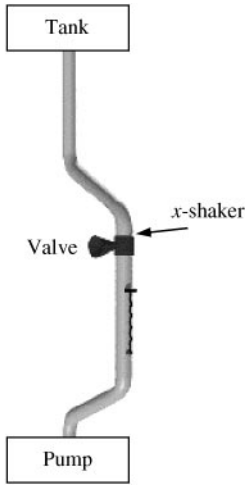

Figure 16. Suction circuit.

the reference by a pump attached to a table at its base and with a tank at the top. The total length of the tested part is about 20 m. A series of tests was done during a block stop, at cold conditions with static fluid inside. The loading was provided by a force F_x following the x-axis, applied just above the valve. The structure was equipped with piezoelectric accelerometers in 10 locations regularly spread over the circuit. Accelerations were collected according to the x direction on the frequency band [0–35 Hz] sampled at steps of 0·0488 Hz. The first five eigenfrequencies, corresponding to eigenmodes outside the plane (yz), are (2·65, 6·46, 8·84, 10·17, 26·42 Hz). The structure was initially modelled by using some straight Timoshenko beams (external diameter of 660·4 mm, wall thickness of 12·7 mm) and circular elbows (same external diameter, wall thickness of 14 mm, curve radius of 0·9906 m, central angle of 65°). The flexibility of the elbow is corrected by dividing their inertias by a coefficient k_f. Only the inertia of the fluid inside the tubes is taken into account by modifying their linear density. Otherwise, the valve is modelled by a 2961 kg lumped mass with an eccentricity of 0·95 m relative to x-axis. The pump and the table are modelled as shown in Figure 17, by a lumped mass (311×10^3 kg) and three lumped stiffnesses k_x^p, $k_{\theta_y}^p$ and

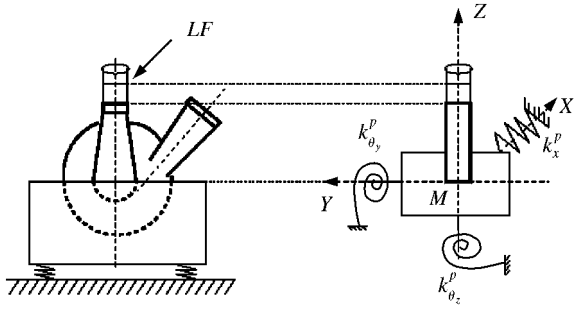

Figure 17. Schematic of the pump connection and of its simplified model.

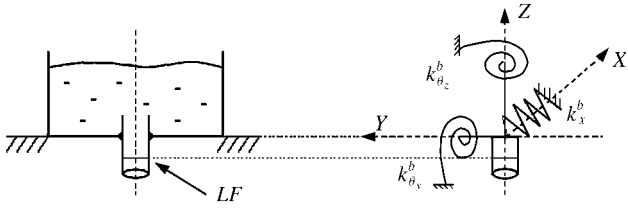

Figure 18. Schematic of the tank connection and of its simplified model.

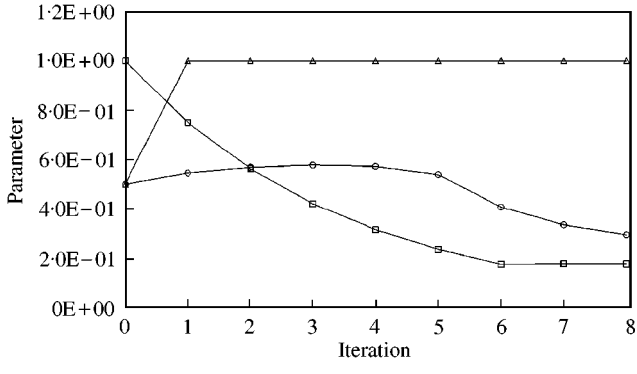

Figure 19. Convergence graph in the suction circuit case. Stiffness of the pump connection (triangle). Stiffness of the tank connection (circle). Elbow flexibility (square).

$k^p_{\theta_x}$. The connection circuit/tank was done by welding the pipe to the bottom of the tank (see Figure 18). It is also modelled by three lumped stiffnesses k^b_x, $k^b_{\theta_y}$ and $k^b_{\theta_x}$. In all results presented here, k^b_x, k^p_x, $k^b_{\theta_y}$ and $k^p_{\theta_x}$ were assumed to be infinite.

The superposition of the frequency responses measured by sensor 2 and obtained by the initial model is shown in the upper graph of Figure 20. A preliminary criterion based on the coherence function between captured signals and the spectrum amplitude of each of them allowed to select 197 frequencies around the various eigenfrequencies. This number was automatically reduced for each iteration if the neighbourhood of a critical frequency appears.

The knowledge of the manufacturing problem and the conception of the various parts of the piping network allowed the choice of the following parameters: p_1 and p_2 associated

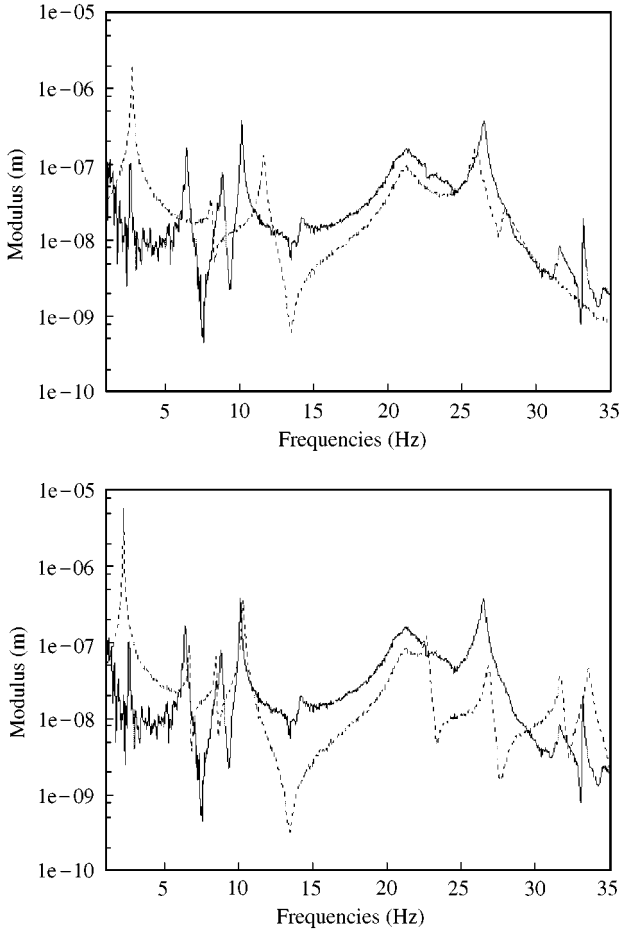

Figure 20. Suction circuit case—comparison between measured and computed responses corresponding to sensor 2. Before updating (upper). After updating (lower).

with $k^p_{\theta_y}$ and $k^b_{\theta_y}$ so that

$$k^p_{\theta_y} = \frac{p_1}{1-p_1}\, k^b_{\theta_{y\,init}}, \quad k^b_{\theta_y} = \frac{p_2}{1-p_2}\, k^b_{\theta_{y\,init}}, \quad k^p_{\theta_{y\,init}} = k^b_{\theta_{y\,init}} = 2{\cdot}83 \times 10^8 \text{ N m},$$

p_3 with the inertia of the four elbows so that

$$I = p_3 I_{init}, \quad I_{init} = 1{\cdot}486 \times 10^{-3} \text{ m}^4.$$

All boundary conditions are modelled and the test degrees of freedom were merged with sensors. Figure 19 shows the resulting convergence graph. For the pump, the updating result was an infinite value for the lumped stiffness $k^p_{\theta_y}$ ($p_1 = 1^-$). This implied that the piping was clamped to the pump. For the connection with the tank, the identified stiffness $k^b_{\theta_y}$ was intermediate between freedom and clamped rotation. This stiffness corresponded to the flexural stiffness of a plate modelling the bottom of the tank. The four elbows were assumed identical in the updating procedure and the coefficient of flexibility obtained for these elbows was 5·5. The French reglementation guide RCC-M suggested a coefficient of

flexibility of 12·43. Bearing in mind that this value is overestimated for the behaviour outside the plane, the value found is realistic.

The comparison of the measured results and the results calculated from the updated model is shown in the lower graph of Figure 20. The resonances identified on the updating model were 2·4, 6·8, 8·5, 10·3 and 28·3 Hz. The first four modes were therefore accurately found. The updated frequencies error were respectively -6, $+6{\cdot}5$, $+3.8$, $+1.3$ and $+7.4\%$. Apart from the amplitude of the first eigenmode which was not well measured due to the very poor coherence at low frequencies, the other amplitudes were almost exact.

5. CONCLUSION

A new approach of parametric updating is presented in this paper. It is based on the measurement of modelling error formulated as a boundary conditions error (BCE). This error is especially well suited to be applied in cases of in-operation structures having unknown boundary conditions such as non-modelled connections or poorly known excitations.

In its principle, the method is based on the choice of a set of degrees of freedom associated with perfectly known boundary conditions. By solving an inverse problem, we therefore construct an image of a modelling error in the form of an error in these boundary conditions. This choice is here supposed to be made in a judicious manner so that the image becomes bijective. This point has not been treated in this paper, but has simply been supposed verified. Of course, this represents a central point when establishing the updating problem, which can not be realized without a well-developed understanding of physics and a minimum knowledge of the tested structure. Another important choice for the efficiency of the objective function is that of the experimental data used for its construction. This point has been treated here. The pertinence of a criteria based on the smallest singular value of the solved system during the identification of the boundary conditions is shown. This criterion depends on the choice of the number and the location of the sensors and the choice of frequencies. The examples presented here show that for a given choice of sensors, this criterion allows determining, and so avoiding, the bands of critical frequencies.

Taking the criterion into account, the efficiency of this new updating technique is shown, allowing identification of the structure parameters in two actual test cases: a laboratory test case and an industrial example.

REFERENCES

1. S. FRIKHA 1992 *Ph.D. Thesis ENSAM, Paris.* Analyse expérimentale des sollicitations dynamiques appliquées à une portion de structure en service modélisable par la théorie des poutres.
2. S. FRIKHA, G. COFFIGNAL and J. L. TROLLE 2000 *Journal of Sound and Vibration* **233**, 495–514. Boundary condition identification using condensation and inversion—application to operating piping network.
3. M. GAUDIN 1996 *Ph.D. Thesis ENSAM, Paris.* Recalage du comportement vibratoire des réseaux de tuyauteries.
4. M. GAUDIN, S. FRIKHA, G. COFFIGNAL and J. L. TROLLE 1998 *Proceedings of the* 16*th International Modal Analysis Conference, Santa Barbara*, 1567–1573. Dynamic updating of piping network using dynamic stiffness matrices.
5. M. I. FRISWELL and J. E. MOTTERSHEAD 1995 *Finite Element Model Updating in Structural Dynamics.* Dordrecht: Kluwer Academic Publishers.
6. N. M. M. MAIA 1998 *Theoretical and Experimental Modal Analysis.* London: Research Studies Press Ltd.

7. D. J. EWINS 1990 *Modal testing Theory and Practice*. London: Research Studies Press Ltd.
8. P. LADEVEZE, D. NEDJAR and M. REYNIER 1994 *American Institute of Aeronautics and Astronautics Journal* **32**, 1485–1491. Updating of finite element model using vibration tests.
9. J. E. MOTTERSHEAD and M. I. FRISWELL 1993 *Journal of Sound and Vibration* **162**, 347–375. Model updating in structural dynamics: a survey.
10. H. G. NATKE 1988 *Probabilistic Engineering Mechanics* **3**, 28–35. Updating computational models in the frequency domain based on measured data: a survey.
11. S. R. IBRAHIM 1990 *Journal of Vibrations and Acoustics* **112**, 107–111. A direct two response approach for updating analytical dynamic model of structure with emphasis on uniqueness.
12. M. W. LESMEZ, D. C. WIGGERT and F. J. HATFIELD 1990 *Transaction of the American Society of Mechanical Engineering, Journal of Fluids Engineering* **112**, 311–318. Modal analysis of vibrations in liquid-filled piping systems.
13. G. H. JAMES, T. G. CARNE and J. P. LAUFER 1995 *International Journal of Analytical and Experimental Modal Analysis* **10**, 260–277. Natural excitation technique (NExT) for modal parameter extraction from operating structures.
14. L. HERMANS and H. V. DER AUWERAER 1997 *Proceedings of the 15th International Modal Analysis Conference, Orlando*, FL. Modal parameter extraction from in-operation data.
15. L. HERMANS and H. V. DER AUWERAER 1999 *Mechanical Systems and Signal Processing* **13**, 193–216. Modal testing and analysis of structures under operating: industrial applications.
16. L. MEVEL, HERMANS and H. V. DER AUWERAER 1999 *Mechanical Systems and Signal Processing* **13**, 823–838. Application of a subspace-based fault detection method to industrial structures.
17. M. ABDELGHANI, M. GOURSAT and T. BIOLCHINI 1999 *Mechanical Systems and Signal Processing* **13**, 839–853. On-line modal analysis monitoring of aircraft structures under unknown excitation.
18. B. PEETERS and G. DE ROECK 1999 *Mechanical Systems and Signal Processing* **13**, 855–878. Reference-based stochastic subspace identification for output-only modal analysis.
19. E. C. PESTEL and F. A. LECKIE 1963 *Matrix Method in Elastomechanics*. New York: McGraw-Hill Book Co.
20. L. MEIROVITCH 1967 *Analytical Methods in Vibrations*. New York: Macmillan.
21. G. H. GOLUB and C. F. VAN LOAN 1990 *Matrix Computation*. New York: Johns Hopkins University Press; second edition. Mathematics/Computer Science.
22. E. WALTER and L. PRONZATO 1994 *Identification de modèles paramétriques à partir de données expérimentales*. Paris: Masson.
23. J. E. DENNIS 1977 *Non Linear Least Squares and Equations—State of the Art in Numerical Analysis*. New York: Academic Press.

APPENDIX A: AN EXAMPLE OF CONTINUOUS ELEMENT TRANSFER AND DYNAMIC STIFFNESS MATRICES AND THEIR DERIVATIVES

One particularity of the method developed in this paper is the use of continuous elements. This allows an exact analytical formulation of the elementary matrices and their derivatives and leads to a small size numerical problem. In order to provide an example of these elementary matrices (see equation (14)), the case of the longitudinal vibrations of a straight beam is detailed here.

Consider a x-axis beam of length l, cross-section area S, density ρ and Young's modulus E. The transfer matrix is derived from the momentum conservation equation and the constitutive law:

$$\frac{\partial N}{\partial x} - \rho S \frac{\partial^2 u}{\partial t^2} = 0, \qquad N - ES \frac{\partial u}{\partial x} = 0.$$

Solving these equations leads to the transfer matrix T_{long}:

$$\begin{Bmatrix} u_2 = u(x = l) \\ N_2 = N(x = l) \end{Bmatrix} = [T_{long}] \begin{Bmatrix} u_1 = u(x = 0) \\ N_1 = -N(x = 0) \end{Bmatrix}$$

with

$$[T_{long}]_{(\omega)} = [D][T^{adim}][D]^{-1} = \begin{bmatrix} 1 & 0 \\ 0 & ESk \end{bmatrix} \begin{bmatrix} \cos kl & -\sin kl \\ -\sin kl & -\cos kl \end{bmatrix} \begin{bmatrix} 1 & 0 \\ 0 & ESk \end{bmatrix}^{-1}.$$

Here the external force convention is used at both extremities of the beam, $k = \omega\sqrt{\rho/E}$ is the wave number and ω is the angular frequency. T^{adim} is the dimensionalless transfer matrix. The dynamic stiffens matrix Z_{long} may be computed from the transfer matrix above provided that $\sin(kl) \neq 0$:

$$Z_{long}(\omega, E) = ESk \begin{bmatrix} \cot kl & \dfrac{-1}{\sin kl} \\ \dfrac{-1}{\sin kl} & \cot kl \end{bmatrix},$$

As an example the updating parameter is assumed to be Young's modulus E. The derivative of the transfer matrix with respect to this parameter is

$$T_{,E} = D_{,E}T^{adim}D^{-1} + DT^{adim}_{,E}D^{-1} - DT^{adim}_{,E}D^{-1}D_{,E}D^{-1},$$

where $X_{,p}$ denotes the derivative of X with respect to p, with

$$T^{adim}_{,E} = k_{,E}T^{adim}_{,k} = \frac{-\omega\sqrt{p}}{2E\sqrt{E}} \begin{bmatrix} -l\sin kl & -l\cos kl \\ -l\cos kl & -l\sin kl \end{bmatrix}$$

and

$$D_{,E} = \begin{bmatrix} 0 & 0 \\ 0 & \dfrac{S\omega}{2}\sqrt{\dfrac{\rho}{E}} \end{bmatrix}.$$

The derivative of the dynamic stiffness matrix with respect to Young's modulus E is

$$Z_{,E} = \frac{S\omega\sqrt{\rho}}{2\sqrt{E}} \begin{bmatrix} \cot g\, kl & \dfrac{-1}{\sin kl} \\ \dfrac{-1}{\sin kl} & \cot kl \end{bmatrix} + \frac{S\omega^2\rho}{2E} \begin{bmatrix} \dfrac{l}{\sin^2 kl} & \dfrac{-l\cos kl}{\sin^2 kl} \\ \dfrac{-l\cos kl}{\sin^2 kl} & \dfrac{l}{\sin^2 kl} \end{bmatrix}.$$

APPENDIX B: NOMENCLATURE

ω	angular frequency
f	frequency
$\{p\}$	updating parameters
$\|u\|_A$	quadratic norm of vector $\{u\}$ according to a weighting matrix $[A]$
$\{q\}$	generalized co-ordinates (linear or angular position, acoustic pressure, etc.)
$\{Q\}$	generalized forces (forces and momentum, acoustical flow, etc.)
$\{q_l\}$	degrees of freedom having an unknown boundary condition
$\{q_t\}$	test degrees of freedom
$\{q_c\}$	clamped degrees of freedom
$\{q_f\}$	free degrees of freedom
$\{Q_l\}$	unknown generalized forces corresponding to an unknown boundary condition
$\{Q_t\}$	generalized forces corresponding to test degrees of freedom
$\{Q_c\}$	reacting generalized forces associated with clamped d.o.f.

$\{Q_f\}$	modelled excitation, generalized forces associated with free d.o.f.
$\{C\}$	measured response
$[T]$	transfer matrix
$[Z]$	dynamic stiffness matrix
SSV	smallest singular values
$X_{,p}$	derivative of X with respect to p